Electrochimica Acta 263 (2018) 346–352

Contents lists available at ScienceDirect

Electrochimica Acta

journal homepage: www.elsevier.com/locate/electacta

Understanding the limits of rapid charging using instrumented commercial 18650 high-energy Li-ion cells

Tazdin Amietszajew*, Euan McTurk, Joe Fleming, Rohit Bhagat

WMG, University of Warwick, Coventry, CV4 7AL, UK

ARTICLE INFO

Article history:
Received 7 September 2017
Received in revised form
16 November 2017
Accepted 11 January 2018
Available online 12 January 2018

Keywords:
Li-ion cell instrumentation
Rapid-charging
Thermal management
Optical fibres
Reference electrode

ABSTRACT

The charging rates of commercial high-energy Li-ion cells are limited by the manufacturer's specifications leading to lengthy charging times. However, these cells are typically capable of much faster charging, if one ensures that the thermal and electrode-specific voltage profiles do not exceed safety limits. Unfortunately, precise and *in-situ* measurements of these parameters have not been achieved to date without altering the operation of these cells. Here we present a method to assess the maximum current for commercial 18650s, using novel instrumentation methods enabling in operando measurements. We found the maximum charging current that could be safely applied to the evaluated high-energy cells is 6.7 times higher than the manufacturer-stated maximum. Subsequently a rapid-charging protocol was developed that leads to over five-fold reduction in charging times without compromising the safety limits of the cells. We anticipate our work to be a starting point for a more sophisticated understanding of commercial Li-ion cells through deployment of diverse *in-situ* sensor systems. This understanding will enable advances in battery materials science, thermal engineering and electrical engineering of battery technology. Furthermore, this work has the potential to help the design of energy storage systems for high performance applications such as motor racing and grid balancing.

1. Introduction

Rechargeable Lithium-ion (Li-ion) cells are widely regarded as the technology of choice for the electrical energy storage and power delivery solutions. With formats ranging from small portable devices to large high energy packs, one of the key applications of this technology is in the automotive industry as a battery pack for electric and hybrid vehicles [1–4]. Fast charging of these batteries is becoming increasingly important as consumers demand reductions in charging time. Concurrently, the applied charging regime has a significant impact on cycle life, thermal performance and safety [5]. Charging guidelines given by cell manufacturers are generally conservative and so significant testing is required before deploying in an application that requires rapid charging.

The most commonly used charging strategy is constant-current constant-voltage (CC-CV), although alternative charging modes are being explored [5–7]. Unfortunately, these attempts are usually lacking experimental *in-situ* thermal measurement or electrode-specific data [7–9]. When assessing the maximum performance limits of the cell, the risk of internal overheating resulting in catastrophic thermal runaway is greatly increased [10]. The commonly agreed five sources of heat generation in Li-ion cells [11] – electrolyte, anode and cathode resistances (R_e, R_a and R_c), anode material and cathode material entropy change (ΔS_a and ΔS_a), can be summarised as Joule (resistive) heating and exothermic reactions [10]. Both of these phenomena are C-rate related and accelerate when a cell experiences heavy load. Subsequently, as the cell temperature increases, the reaction rates for the decomposition of the electrolyte increase, which can lead to the electrolyte breakdown and gas formation, resulting in pressure build-up in the cell [12]. Additionally, if a cell is charged too fast, lithium metal can electroplate on the anode, which may grow in the form of dendrites and eventually pierce the separator, causing an internal short circuit and subsequent catastrophic failure [13]. This is most pronounced in the case of high-energy cells which, while providing significantly more gravimetric and volumetric energy density than their high-power counterparts, suffer from significantly limited charge rates [14,15].

To be able to overcome these obstacles, information about each electrode's potential is required, complemented by the surface and internal thermal load responses of the cell. Here we use a novel

* Corresponding author.
E-mail address: T.Amietszajew.1@warwick.ac.uk (T. Amietszajew).

https://doi.org/10.1016/j.electacta.2018.01.076

instrumentation design for commercial 18650 cells that minimises the adverse and previously unavoidable alterations to the cell geometry [16]. This includes an *in-situ* reference electrode coupled with an optical fibre temperature sensor. This enables the measurement of each electrode's potential, supplemented by the cell's internal and external temperature profiles. In addition to performance and safety optimisation, monitoring of internal cell temperature and each electrode potentials can be an important asset when trying to minimise aging effects and enable degradation effects early onset detection, e.g. by observing the negative electrode voltage slippage as the cell ages [17]. Introduction of a reference electrode was previously attempted by other researchers on Li-ion pouch and cylindrical cells [18–20]. The latter was more challenging due to assembly constraints, often resulting in extensive modification of the cell which can affect its internal resistance and electrolyte stability.

In-situ thermal instrumentation of Li-ion cells using thermocouples has been explored by other researchers [21–23]. However, this technology has intrinsic limitations that restrict its applicability. Thermocouples measure only relative temperature changes, therefore requiring a cold junction element and extra calibration. A thermocouple is not capable of multiplexing to a single wire, which means additional signal lines are required, thickening the sensor and adding points of failure to obtain distributed sensing. Conversely, FBG sensors support multiplexing using a single fibre thread with multiple gratings. Finally, the sensitivity of thermocouples is relatively low, requiring additional analogue conditioning circuits. Therefore, fibre optic temperature sensors are evaluated instead as a more promising alternative.

In this work, we use the instrumented Li-ion cell to assess the maximum charging current for the commercial 18650 high-energy cell and derive expedient charging parameters which remain within the thermal and potential safety limits of the cell. The approach utilised offers an unprecedented insight into the performance characteristics of the cell, allowing a much better understanding of actual electrochemical and thermal limitations of Li-ion batteries for the benefit of scientists researching new battery materials and engineers designing electric vehicle and grid storage systems.

2. Experimental

2.1. Cell instrumentation – reference electrode

Lithium metal foil was used as an in-situ reference electrode. Bare metal reference electrodes called quasi-references are often used in certain situations when it is impossible to introduce standard references due to mechanical [24] and/or chemical [25] constraints [26]. Lithium metal electrodes were previously reported to work successfully in pouch cells, where the geometry of the pouch cell format allows for easier modification [27]. This is due to the soft, flexible pouch material, which can accommodate additional elements inside the cells, while the electrodes in cylindrical cells are surrounded by a stiff metal can. Additionally, pouch cells have a substantially sized and easily accessible flat area at the top and bottom of the electrode stack, while cylindrical cells are built with very tightly wound electrodes - this allows for the reference placement only at the top of the jellyroll, and also requires the metal can to be cut open for cell modification.

As lithium metal reference electrodes can suffer from polarizability at high current densities, bespoke lithium titanate and lithium iron phosphate reference electrodes were also evaluated by other researchers [28,29]. In this work, a high-impedance input connection to the potentiostat is used to prevent any current from passing through the electrode, while maintaining the simplicity of the design and preventing any new foreign materials from influencing the system [26].

A strip of Li foil was used, wrapped in separator material to prevent it short-circuiting against the cell can or the electrode jellyroll, subsequently disturbing and reacting with the electrode materials. The electrode was then inserted into the top of the cylindrical cell, below the cathode cap, in contact with the cell's jelly roll. A spacer made from Kapton tape was placed on the upper side of the reference electrode to ensure good ionic contact with the jelly roll and prevent shorting with the cathode current collector once assembled inside the cell. After the modification procedure, the anode, cathode and full cell potentials were monitored for 24 h to confirm stability of the modified cell and the reference electrode readings. This setup allows for simultaneous observation of the cathode and anode potentials of a working Li-ion cell *vs.* Li/Li^+.

2.2. Cell instrumentation – thermal sensors

The selected thermal sensing method involves the use of Fibre Bragg Gratings (FBG) [30]. The FBG element was obtained from *Smart* Sensors Inc. in its bare form, sealed with a polyamide recoat stable in a temperature range of −270 °C to +300 °C. The element has a nominal wavelength of 1545 nm at 25 °C when no strain is applied. The bare fibre was then threaded through an aluminium tube, forming a strain protection layer. An outer skin of fluorinated ethylene propylene heat-shrink was applied over the fibre and aluminium, adding protection from the electrolyte. Elements prepared in such a way can withstand electrical, chemical and mechanical stress inflicted during the instrumentation procedure and during cycling. Fig. 1 shows the complete element.

An optical spectrum analyser, broadband laser source and a three port optical circulator (*Thor Labs Inc.*) were used to interrogate the wave shift of the FBG. The analyser was subsequently connected *via* RS-232 to a data logging computer. The observed wave shift was being translated to a temperature shift using an equation specific to a given FBG element based on its sensitivity

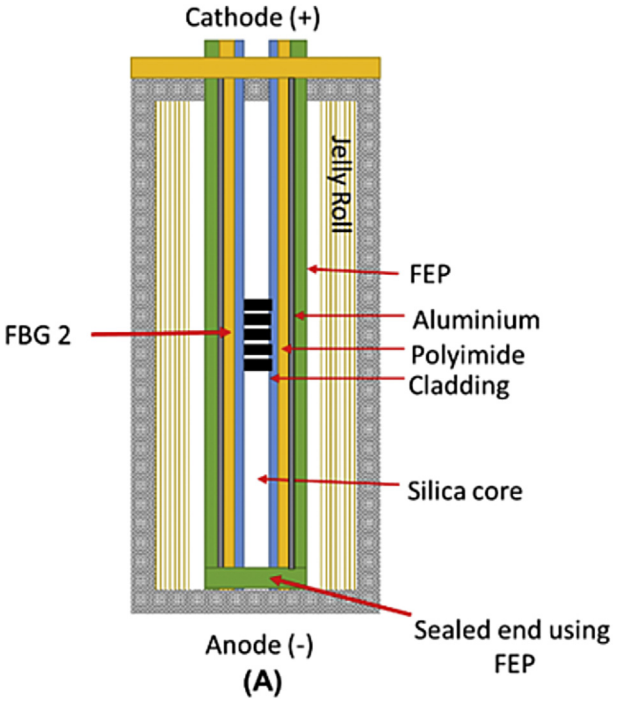

Fig. 1. Schematics of the FBG sensing element embedded into a Li-ion cylindrical cell.

factor, enabling real time temperature monitoring. A separate thermocouple data logging unit (Pico Technology®) was used to log the ambient and cell can surface temperature. The FBG elements and thermocouple were subject to a single-point calibration, using a high accuracy platinum resistance temperature detector (RTD) PT100 (Pico®) with a UKCAS accredit test certificate. The experiments were conducted in a temperature-controlled environment at 25 ± 0.1 °C.

2.3. Cell instrumentation – cell assembly

Commercial 18650 high-energy cells with nickel cobalt aluminium (NCA) cathode chemistry were used for this study. Other cell formats could also be evaluated using the same sensors, subject to their specific geometric restrictions. With nominal voltage of 3.6 V and 3 Ah rated capacity, the cells weighed ~50 g. The evaluated cells were opened at the cathode end using a pipe cutter inside an argon glove box with O_2 and H_2O concentrations of <0.1 ppm. A pre-assembled reference electrode was placed on top of the electrode jellyroll, after which the cathode cap was placed back on top of the cell. The cell was re-sealed using Kapton tape and epoxy resin. For cells instrumented with a thermal sensor, a hole was punched in the cathode cap for the thermal sensor to be inserted through the cap into the mandrel core, locating the temperature sensor in the middle of the cell. The opening was subsequently sealed with silicone. A complementary temperature sensor was placed on the outside of a cell can. Key advantages of these designs include no chemical or mechanical alteration to the jelly roll, thus preventing changes in SEI formation or internal resistance; excellent ionic contact between reference electrode and both the anode and cathode, thus ensuring stable electrode potential readings; with scope for high-resolution temperature readings across the length of the cell core using the fibre sensors.

2.4. Cell cycling

The cell cyclers used for this experimentation were *BioLogic VMP3* channels with 5 A or 10 A boosters, depending on the current required, and a *Princeton VersaSTAT* potentiostat with a 10 A booster. Cyclers were controlled using EC-Lab® or VersaStudio. The optical fibre sensor was interrogated using an *Aq6370 Yokogawa* optical spectrum analyser with a broadband laser source. The recorded wave shift was subsequently translated into temperature changes. All of the data gathered was analysed and plotted using *MatLab*® analytical software.

18650 high-energy cylindrical cells were initially cycled with constant currents, which were progressively increased whilst observing the thermal and reference electrode responses in order to avoid thermal runaway and electrode damage. The standard discharge current used was 3 A, which equates to 1C. The resulting data obtained is shown in Figs. 2 and 3.

Three prototype rapid-charging regimes were evaluated, based on the data obtained from the aforementioned tests. As the risk of cell degradation and lithium plating is enhanced at higher SoC [7], the charging current in each rapid charging procedure was gradually decreased in steps based on SoC and operating voltage. The evaluated procedures are called Rapid 1, 2 and 3, and are outlined in Table 1. The resulting data obtained is shown in Figs. 4 and 5. Each rapid charging procedure was applied for at least 50 cycles. Rapid 1 consists of 6 A for 1.5 Ah, 4.5 A for 0.5 Ah, then 3 A, 1.8 A and 0.9 A until each reached 4.2 V, followed by CV at 4.2 V. All of the CC steps had a 30 s break between them to allow the cell reaction kinetics, chiefly the Warburg diffusion to catch up and thus allow the cell potential to relax slightly before the next step, to avoid instances of steps terminating by prematurely hitting the voltage limits. Rapid 2 was 6 A for 1 Ah, 4.5 A for 1 Ah, then 3 A, 1.8 A and 0.9 A until 4.2 V, followed by CV at 4.2 V. Finally, Rapid 3 applied 5 A for 1.5 Ah, 4 A for 0.5 Ah, then 3 A, 1.8 A and 0.9 A until 4.2 V, followed by CV at 4.2 V. All the CV steps followed 60 mA as the current cut-off point.

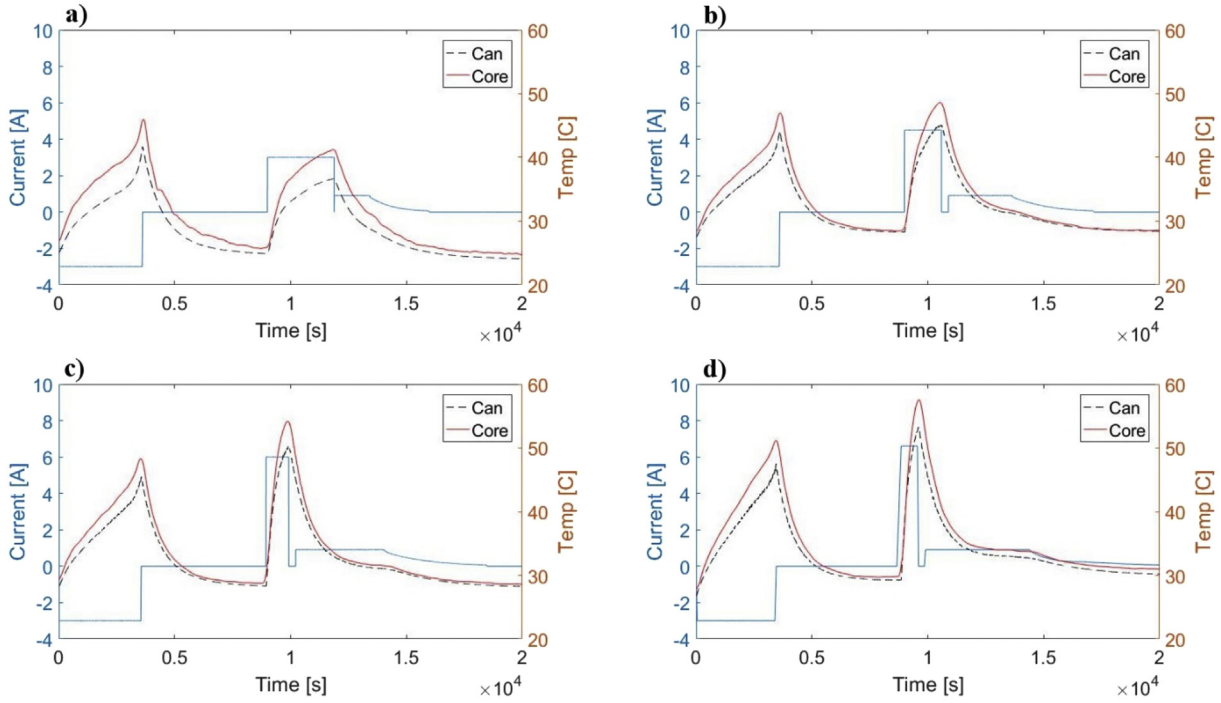

Fig. 2. Cell thermal response to charging using high constant currents, preceded by a 1C (3A) discharge. The rates used were as follows: a) 1C, b) 1.5C, c) 2C, d) 2.2C. As the cells' specified capacity is 3 Ah, 1C corresponds to 3 A current. As the manufacturer-stated 60 °C thermal limit was approached at 2.2C (6.6A), no higher currents were evaluated.

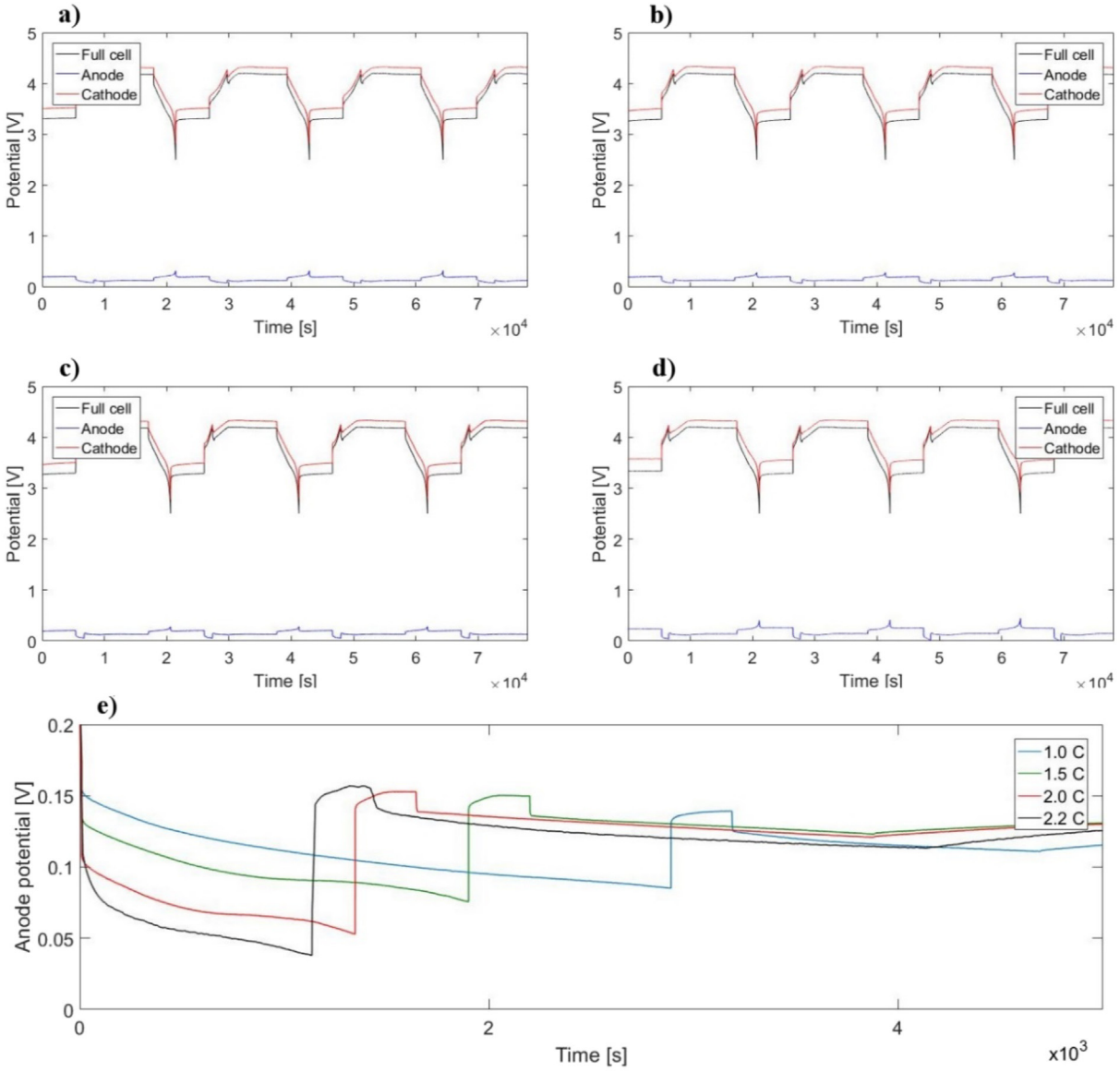

Fig. 3. Cell 3-electrode potential response to charging using high constant currents. The rates used were as follows: a) 1C, b) 1.5C, c) 2C, d) 2.2C. e) insert shows anode responses to the applied currents. As the cells' specified capacity is 3Ah, 1C corresponds to 3A. Cathode and anode potentials are reported vs. Li/Li^+ reference.

Table 1
Evaluated charging profiles.

Step	CC charge 0–80% followed by CC-CV		Rapid 1		Rapid 2		Rapid 3	
Header limit for all steps: 4.2 V, 60 °C								
	Current (A)	Additional Limit	Current (A)	Additional Limit	Current (A)	Additional Limit	Current (A)	Additional Limit
1	3/4.5/6/6.6	2.4 Ah	6	1.5 Ah	6	1 Ah	5	1.5 Ah
2	0	30 s (rest)	0	30 s (rest)	0	30 s (rest)	0	30 s (rest)
3	0.9	0.06 A	4.5	0.5 Ah	4.5	1 Ah	4	0.5 Ah
4			0	30 s (rest)	0	30 s (rest)	0	30 s (rest)
5			3		3		3	
6			0	30 s (rest)	0	30 s (rest)	0	30 s (rest)
7			1.8		1.8		1.8	
8			0	30 s (rest)	0	30 s (rest)	0	30 s (rest)
9			0.9	0.06 A	0.9	0.06 A	0.9	0.06 A

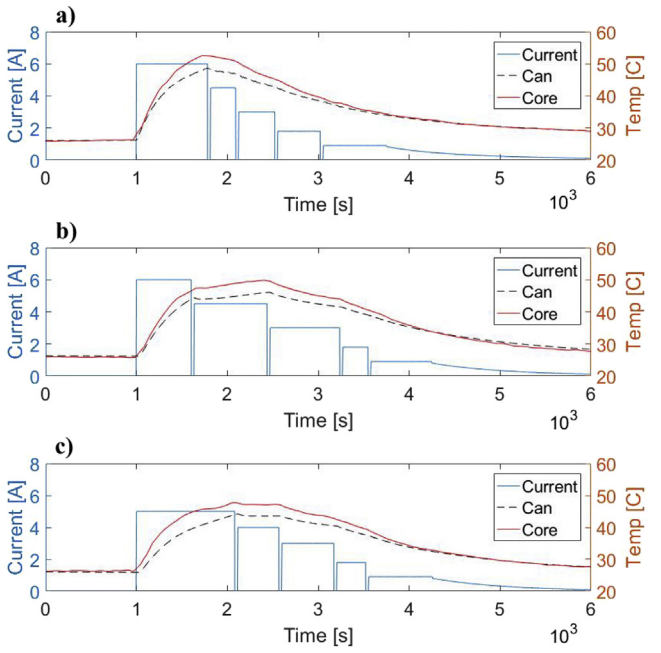

Fig. 4. Cell thermal responses to the evaluated rapid charge protocols. The modes used, a) Rapid 1, b) Rapid 2 and c) Rapid 3, are described in Table 1. Lower peak temperature can be observed for slower charging regimes.

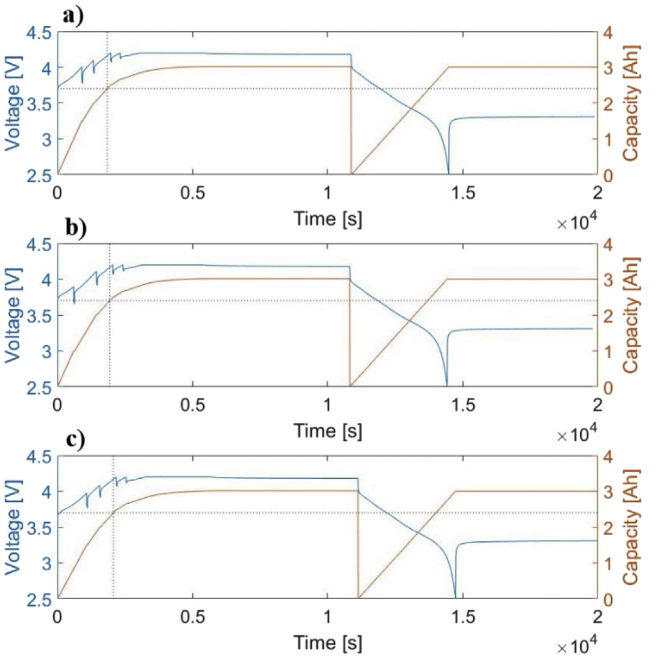

Fig. 5. The potential and capacity profiles of rapid charging modes; a) Rapid 1, b) Rapid 2 and c) Rapid 3, described in detail in Table 1. The dotted line represents 80% SoC. The charging times increase slightly when using the latter charging profiles, highlighting the trade-off between performance and approaching thermal and potential safety limits.

3. Results and discussion

3.1. Thermal and electrochemical evaluation of high-current cell charging

High-energy Nickel-Cobalt-Aluminium (NCA) Li-ion cylindrical 3 Ah 18650 cells were instrumented and cycled in a temperature-controlled test chamber at 25 °C. The cells were initially charged at constant current, which was progressively increased whilst observing the internal thermal and individual electrode responses. The specific current evaluated was applied from 0% to 80% State of Charge (SoC), followed by the standard constant-current constant-voltage (CC-CV) mode as stated in the manufacturer's specification, i.e. 0.9 A CC and subsequent CV at 4.2 V with 60 mA current cut-off criterion. The standard discharge current used was 3 A (1 C). The cycling regimes evaluated are summarised in Table 1.

Thermal data for the instrumented cells is shown in Figs. 2 and 4. The full cell, anode and cathode electrochemical potentials data is presented in Figs. 3 and 5. Anode and cathode potentials are reported *vs.* Li/Li^+ reference. Firstly the data is presented for the single high current CC charging procedures, and subsequently for the Rapid charging procedures created based on the prior testing.

As shown in Fig. 2a–d, the surface and core temperatures of the cell increase concurrently with charging currents. This is due to the previously described Joule (ohmic) heating as well as a number of exothermic electrochemical reactions occurring during the cell operation [31]. Increasing the rate of these as well as through faster resistive heat generation causes the observed temperature rise. These effects are an unavoidable part of the cell operation and have to be evaluated for each cell design – some manufacturers attempt to reduce the heat accumulation e.g. by using less resistive current collectors or external cooling [32]. The evaluated cells core temperature increased from the region of 40 °C at 1 C (3 A) in Fig. 1a, to 60 °C at 2.2 C (6.6 A) in Fig. 2d. As previously described, 60 °C is the manufacturer-specified temperature safety limit for this cell, above which electrolyte decomposition is accelerated and there is a significant increase in risk of thermal runaway through a chain of exothermic reactions [10]. Therefore, a charging rate of 2.2 C was concluded as bringing the cell too close to thermal abuse conditions. Importantly, the core temperature of the cell was 5 °C higher than the external can temperature during all of the rapid charges that were investigated. This underlines the necessity of core temperature observation when developing cell usage guidelines, as the variation between the can and the core is significant in the case of cylindrical cells, as evaluated here.

In this study, higher constant currents were terminated at an SoC of no more than 80% in order to limit the temperature increase, prevent anodic lithium plating and avoid driving the polarised cathode potential to a value that would cause a degradation as the cell approached 100% SoC. This is due to the fact that cells exhibit increased internal resistance at higher SoC, resulting in higher overpotentials and heat generation [7]. Consequently, charging at higher SoC requires lower currents to be applied in order to avoid cell damage due to the greater overpotential encountered which can result in voltage limits being exceeded. For this reason, the charge ends with the constant-voltage control phase, during which the charging current tapers off to a specified limit. This is the least time-efficient part of the charge protocol [7]. Despite these concerns, it can be seen that the 1 C charge (Fig. 2a) from 0% to 80% SoC reached a lower maximum temperature than the preceding discharge from 100% to 0% SoC, indicating that this cell can be charged with currents higher than 1C without breaching the temperature safety limits in its core. However, it should to be noted that out of the four charge rates evaluated, only cells charged at 1 C were able to charge to 80% SoC before reaching the full cell voltage limit of 4.2 V. This shows that using only a high constant current to achieve a full charge of a cell would not work, and underlines the importance of the development of tailored rapid charging protocols.

The electrode potentials shown in Fig. 3 allow for electrode-specific analyses of the processes occurring in the cell. As there is a risk of lithium metal plating [5] on the negative electrode during

charging it is important to ensure that the negative electrode potential does not reach 0 V vs Li. Such a low potential would indicate that it has become electrochemically favourable for metallic lithium to deposit on the anode surface. Fig. 1e shows an enhanced view of the anode potentials for each rate. It can be seen that as the current rate increases, the anode voltage decreases, ultimately dropping below 0.05 V for 2.2 C (6.6 A). This, combined with thermal profiles showing that the cell core reached 60 °C at 2.2 C, suggested that the highest charge rate used for the developed rapid charge procedures should be 2 C.

3.2. Rapid charging protocols development

Given the observations above, the three rapid charging protocols developed were based on progressively reducing the applied current as the cells charged, also known as derating, followed by a final CC-CV profile to 100% SoC. The protocols evaluated are described in greater detail in Table 1. The applied charge currents and the resulting thermal profiles are shown in Fig. 4. The corresponding full cell, anode and cathode potentials are presented in Fig. 5. A rapid charging procedure was only deemed successful if the cell core temperature remained less than 60 °C (temperature limit outlined by the manufacturer), and the negative electrode potential more than 0 V, for the entire charge procedure.

The temperature profiles show direct correlation to the applied currents. The most significant rate of temperature increase is recorded during the 6 A period (Fig. 4a), and is less so when applying 5 A (Fig. 4c). The subsequent 4.5 A step causes less pronounced temperature increase in the case of Rapid 2 (Fig. 4b) charge, while for Rapid 1 protocol (Fig. 4a) the cell starts to cool down. This is due to the heat dissipation [33] following the longer 6 A segment in Rapid 1 (Fig. 4a) being greater than the heat generated during the 4.5 A step; the thermal equilibrium would be lower if 4.5 A was applied from the start of the procedure. Conversely, the shorter 6 A segment of Rapid 2 (Fig. 4b) does not exceed this thermal equilibrium, and so the cell temperature continues to rise when 4.5 A is applied. The successive derating stages of the rapid charge protocols enable the cells to cool down further, while still supplying significant currents. The lower current stages (3 A, 1, 8 A and 0.9 A) are limited by cell voltage, as explained in Table 1. The stepped current pattern displayed in Fig. 3 results in the serrated voltage pattern shown in Fig. 5.

Fig. 5 indicates that most of the charge is delivered to the cell during the stepped CC part of the charging protocol. Importantly, we were able to achieve a constant-current phase during charge that continues beyond 80% SoC without resulting in the anode potential reaching 0 V vs Li, thus indicating that the voltage limit of the cell was not exceeded during the attainment of this target SoC. It is also evident that the cell voltage increases rapidly when high currents are applied, which highlights the importance of the intermediate rest periods between the high current phases allowing the cell potential to relax [34] sufficiently before the next derated current phase, avoiding exceeding the cell's voltage limits. Such a phenomenon is related to the limited rate of lithium diffusion into the anode microstructure [35–37]. If the applied current exceeds the lithium diffusion rate, it would lead to lithium plating on the negative electrode. This issue underlines the need for anode potential monitoring during rapid charging protocols evaluation. The approach in this work allows for the application of a series of high currents without reaching the electrochemical or thermal safety limits of the cell. Accordingly, the charging times achieved are significantly shorter than the cell supplier's standard charging protocol, as shown in Table 2.

Each of the evaluated rapid charging procedures charges the cell from 0% to 80% SoC in under 35 min. However, each procedure takes twice as long to charge the cell the remaining 20%–100% SoC. This is due to the previously discussed phenomenon of internal resistance increase at higher SoCs, which subsequently limits the current that can be safely applied to the cell [7]. Columbic efficiency, i.e. proportion of charge stored to charge delivered, is measured at approximately at 99.5% when the evaluated rapid charging modes are applied. This is related to a proportion of the energy used being spent on heat generation and parasitic reactions leading to capacity loss [38], including electrolyte decomposition and localised lithium plating, the latter however minimised as much as possible by avoiding the anode potential dropping too close to 0 V. Consequently, the capacity loss was measured at 0.2% per cycle over the first hundred cycles. This indicates that, while the evaluated rapid charging procedures can offer over fivefold reduction in charge time over the standard charge protocol, the rate of capacity loss encountered should be factored into cell management in real-world applications to minimise its impact. This could be achieved, for example, by alternating rapid and standard charging procedures [7], depending on the use scenario, or limiting the rapid charging application to on-demand cases when required. Nonetheless, this work demonstrates some powerful *in-situ* analytical tools that can be used to develop and refine cell cycling protocols and determine the true limits of the cell with respect to maximisation of performance while meeting safety requirements.

Table 2
Comparison of charging times of the evaluated rapid charging procedures vs. standard charging.

Charging mode	80% SoC	100% SoC
Standard	2h 39min 46s	3h 55min 30s
Rapid 1	30min 41s	1h 30min
Rapid 2	32min 12s	1h 30min
Rapid 3	34min 28s	1h 35min

4. Conclusions

The objective of this study was to evaluate new methods to assess the limits of high-energy Li-ion cells rapid charging, using smart instrumented commercial 18650 cylindrical cells. Both thermal and electrochemical responses from inside the cell were successfully monitored under various constant charging currents, enabling us to deepen the understanding of the real performance and safety limits of the cell. A difference of up to 5 °C was detected between the core and can temperature of the evaluated 18650 cylindrical cells; this is a disparity which should be considered when determining cell safety limits and usage guidelines. The highest charging current applied without breaching the electrochemical and manufacturer-specified thermal safety limits was 6 A, which equals a rate of 2 C for the evaluated cell and is 6.7 times higher than the manufacturer-stated maximum current. This shows the significance of possible performance optimisations that can be made to the cycling protocols for commercially available cells through the use of smart instrumentation and analysis.

The data gathered using the instrumented cells enabled the creation of a tailored rapid charging profile. The charge from 0% to 80% SoC was accelerated five times over the standard procedures, greatly improving the availability of a device powered by such cells. This work validated the developed current-derating rapid charging procedure as feasible and safe for high-energy cells which commonly suffer from long charging times, although with a somewhat adverse effect on the cell long-term capacity retention if used as the main charging protocol, which should be factored into the cell management. Furthermore, the cell instrumentation techniques developed for this study have been shown to be valuable

tools for assessing the true operational limits of commercial Li-ion cells, enabling considerably greater performance to be harnessed from present-day and future cell chemistries, without jeopardising safety.

Author contributions

T.A. and E.M-T. performed the experiments with assistance of J.F. T.A. analysed the data with assistance of J.F. R.B. supervised the project. All authors wrote the manuscript.

Competing financial interests

The authors declare no competing financial interests.

Data availability

The datasets generated and analysed during the current study are available from the corresponding author on request, but some restrictions apply to the availability of the data on the commercial cells used for this study.

Acknowledgments

The work outlined above was carried out as part of AMPLIFII, a collaborative research project supported by Innovate UK & UK Government Office for Low Emission Vehicle (contract reference 102490). The project consortium includes the University of Warwick (coordinator), Alexander Dennis Limited, Ariel Motor Company Limited, Augean plc, Axion Consulting Limited, Delta Motorsport, HORIBA MIRA Limited, Jaguar Land Rover Limited, JCB Service, Potenza Technology Limited, Trackwise Designs Limited and the University of Oxford.

References

[1] A. Opitz, P. Badami, L. Shen, K. Vignarooban, A.M. Kannan, Can Li-Ion batteries be the panacea for automotive applications? Renew. Sustain. Energy Rev. 68 (2017) 685–692, https://doi.org/10.1016/j.rser.2016.10.019.
[2] B. Nykvist, M. Nilsson, Rapidly falling costs of battery packs for electric vehicles, Nat. Clim. Change 5 (2015) 329–332, https://doi.org/10.1038/nclimate2564.
[3] P. Miller, Automotive lithium-ion batteries, Johnson Matthey Technol. Rev. 59 (2015) 4–13, https://doi.org/10.1595/205651315X685445.
[4] B. Scrosati, J. Garche, Lithium batteries: status, prospects and future, J. Power Sources 195 (2010) 2419–2430, https://doi.org/10.1016/j.jpowsour.2009.11.048.
[5] P. Keil, A. Jossen, Charging protocols for lithium-ion batteries and their impact on cycle life-An experimental study with different 18650 high-power cells, J. Energy Storage 6 (2016) 125–141, https://doi.org/10.1016/j.est.2016.02.005.
[6] C.H. Lin, C.L. Chen, Y.H. Lee, S.J. Wang, C.Y. Hsieh, H.W. Huang, K.H. Chen, Fast charging technique for Li-Ion battery charger, in: Proc. 15th IEEE Int. Conf. Electron. Circuits Syst. ICECS 2008, 2008, pp. 618–621, https://doi.org/10.1109/ICECS.2008.4674929.
[7] P.H.L. Notten, J.H.G.O.H. Veld, J.R.G. Van Beek, Boostcharging Li-ion batteries: a challenging new charging concept, J. Power Sources 145 (2005) 89–94, https://doi.org/10.1016/j.jpowsour.2004.12.038.
[8] D. Anseán, M. González, J.C. Viera, V.M. García, C. Blanco, M. Valledor, Fast charging technique for high power lithium iron phosphate batteries: a cycle life analysis, J. Power Sources 239 (2013) 9–15, https://doi.org/10.1016/j.jpowsour.2013.03.044.
[9] A. Abdollahi, X. Han, G.V. Avvari, N. Raghunathan, B. Balasingam, K.R. Pattipati, Y. Bar-Shalom, Optimal battery charging, Part I: minimizing time-to-charge, energy loss, and temperature rise for OCV-resistance battery model, J. Power Sources 303 (2016) 388–398, https://doi.org/10.1016/j.jpowsour.2015.02.075.
[10] Q. Wang, P. Ping, X. Zhao, G. Chu, J. Sun, C. Chen, Thermal runaway caused fire and explosion of lithium ion battery, J. Power Sources 208 (2012) 210–224, https://doi.org/10.1016/j.jpowsour.2012.02.038.
[11] R. Srinivasan, A. Carson Baisden, B.G. Carkhuff, M.H. Butler, The five modes of heat generation in a Li-ion cell under discharge, J. Power Sources 262 (2014) 93–103, https://doi.org/10.1016/j.jpowsour.2014.03.062.
[12] I. Bloom, S.A. Jones, E.G. Polzin, V.S. Battaglia, G.L. Henriksen, C.G. Motloch, R.B. Wright, R.G. Jungst, H.L. Case, D.H. Doughty, Mechanisms of impedance rise in high-power, lithium-ion cells, J. Power Sources 111 (2002) 152–159.
[13] D. Deng, Li-ion batteries: basics, progress, and challenges, Energy Sci. Eng. 3 (2015) 385–418, https://doi.org/10.1002/ese3.95.
[14] P.V. Braun, J. Cho, J.H. Pikul, W.P. King, H. Zhang, High power rechargeable batteries, Curr. Opin. Solid State Mater. Sci. 16 (2012) 186–198, https://doi.org/10.1016/j.cossms.2012.05.002.
[15] K.E. Aifantis, S.A. Hackney, V. Kumar, High Energy Density Lithium Batteries: Materials, Engineering, Applications, Wiley-VCH Verlag GmbH & Co. KGaA, 2010, https://doi.org/10.1002/9783527630011.
[16] P. Liu, J. Wang, J. Hicks-Garner, E. Sherman, S. Soukiazian, M. Verbrugge, H. Tataria, J. Musser, P. Finamore, Aging mechanisms of LiFePO[sub 4] batteries deduced by electrochemical and structural analyses, J. Electrochem. Soc. 157 (2010) A499, https://doi.org/10.1149/1.3294790.
[17] X. Han, M. Ouyang, L. Lu, J. Li, Y. Zheng, Z. Li, A comparative study of commercial lithium ion battery cycle life in electrical vehicle: aging mechanism identification, J. Power Sources 251 (2014) 38–54. https://doi.org/10.1016/j.jpowsour.2013.11.029.
[18] T. Osaka, D. Mukoyama, H. Nara, Review—development of diagnostic process for commercially available batteries, especially lithium ion battery, by electrochemical impedance spectroscopy, J. Electrochem. Soc. 162 (2015) A2529–A2537, https://doi.org/10.1149/2.0141514jes.
[19] J.R. Belt, D.M. Bernardi, V. Utgikar, Development and use of a lithium-metal reference electrode in aging studies of lithium-ion batteries, J. Electrochem. Soc. 161 (2014) A1116–A1126, https://doi.org/10.1149/2.062406jes.
[20] G. Nagasubramanian, Two- and three-electrode impedance studies on 18650 Li-ion cells, J. Power Sources 87 (2000) 226–229, https://doi.org/10.1016/S0378-7753(99)00469-3.
[21] G. Zhang, L. Cao, S. Ge, C.-Y. Wang, C.E. Shaffer, C.D. Rahn, In Situ measurement of radial temperature distributions in cylindrical Li-Ion cells, J. Electrochem. Soc. 161 (2014) A1499–A1507, https://doi.org/10.1149/2.0051410jes.
[22] M.S.K. Mutyala, J. Zhao, J. Li, H. Pan, C. Yuan, X. Li, In-situ temperature measurement in lithium ion battery by transferable flexible thin film thermocouples, J. Power Sources 260 (2014) 43–49, https://doi.org/10.1016/j.jpowsour.2014.03.004.
[23] T. Waldmann, G. Bisle, B.I. Hogg, S. Stumpp, M.A. Danzer, M. Kasper, P. Axmann, M. Wohlfahrt-Mehrens, Influence of cell design on temperatures and temperature gradients in lithium-ion cells: an in Operando study, J. Electrochem. Soc. 162 (2015) A921–A927, https://doi.org/10.1149/2.0561506jes.
[24] T. Amietszajew, S. Sridhar, R. Bhagat, Metal recovery by electrodeposition from a molten salt two-phase cell system, J. Electrochem. Soc. 163 (2016) D515–D521, https://doi.org/10.1149/2.0991609jes.
[25] Y. Wen, X. Wang, Characterization and application of a metallic tungsten electrode for potentiometric pH measurements, J. Electroanal. Chem. 714–715 (2014) 45–50, https://doi.org/10.1016/j.jelechem.2013.12.031.
[26] A. Lewenstam, F. Scholz, Handbook of Reference Electrodes, Springer Berlin Heidelberg, Berlin, Heidelberg, 2013, https://doi.org/10.1007/978-3-642-36188-3.
[27] E. McTurk, C.R. Birkl, M.R. Roberts, D.A. Howey, P.G. Bruce, Minimally invasive insertion of reference electrodes into commercial lithium-ion pouch cells, ECS Electrochem. Lett. 4 (2015), https://doi.org/10.1149/2.0081512eel.
[28] F. La Mantia, C.D. Wessells, H.D. Deshazer, Y. Cui, Reliable reference electrodes for lithium-ion batteries, Electrochem. Commun. 31 (2013) 141–144, https://doi.org/10.1016/j.elecom.2013.03.015.
[29] D. Juarez-Robles, C.-F. Chen, Y. Barsukov, P.P. Mukherjee, Impedance evolution characteristics in lithium-ion batteries, J. Electrochem. Soc. 164 (2017) A837–A847, https://doi.org/10.1149/2.1251704jes.
[30] S. Dewra, V. Grover, A. Grover, Fabrication and application of fiber Bragg grating - a review, Adv. Eng. Technol. Appl. 4 (2015) 15–25.
[31] S.J. Drake, M. Martin, D.A. Wetz, J.K. Ostanek, S.P. Miller, J.M. Heinzel, A. Jain, Heat generation rate measurement in a Li-ion cell at large C-rates through temperature and heat flux measurements, J. Power Sources 285 (2015) 266–273, https://doi.org/10.1016/j.jpowsour.2015.03.008.
[32] G.-H. Kim, A. Pesaran, Battery thermal management system design modeling, in: 22nd Int. Batter. Hybrid Fuel Cell Electr. Veh. Conf. Exhib. EVS22, vol. 1, 2006, pp. 126–133. http://zanran_storage.s3.amazonaws.com/www.nrel.gov/ContentPages/184201983.pdf.
[33] J. Crank, The Mathematics of Diffusion, Oxford University Press, Oxford, 1975.
[34] P.A. Nelson, K.G. Gallagher, I. Bloom, D.W. Dees, Modeling the Performance and Cost of Lithium-ion Batteries for Electric-drive Vehicles, Oak Ridge, TN, 2012.
[35] E.V. Thomas, I. Bloom, J.P. Christophersen, V.S. Battaglia, Rate-based Degradation Modeling of Lithium-ion Cells, 2012.
[36] K. White, R.T. Long, Lithium-ion Batteries Hazard and Use Assessment, Quincy, Massachusetts, 2011.
[37] R. Alcantara, P. Lavela, C. Perez-Vincente, J.L. Tirado, Anode materials for lithium-ion batteries, in: Lithium Ion Batter. Adv. Mater. Technol, 2012, pp. 97–146.
[38] C.R. Birkl, M.R. Roberts, E. Mcturk, P.G. Bruce, D.A. Howey, Degradation diagnostics for lithium ion cells, J. Power Sources 341 (2016) 1–35, https://doi.org/10.1016/j.jpowsour.2016.12.011.